Communication

Surface-Charge Induced Ion Depletion and Sample Stacking near Single Nanopores in Microfluidic Devices

Kaimeng Zhou, Michelle L. Kovarik, and Stephen C. Jacobson

J. Am. Chem. Soc., **2008**, 130 (27), 8614-8616 • DOI: 10.1021/ja802692x • Publication Date (Web): 13 June 2008

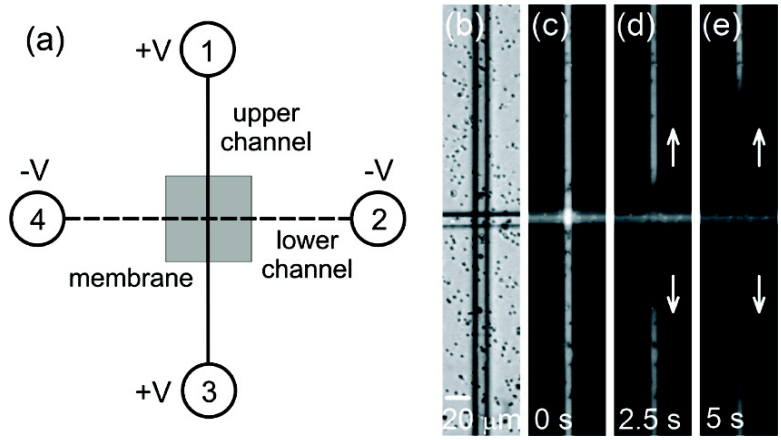

More About This Article

Additional resources and features associated with this article are available within the HTML version:

- Supporting Information
- Links to the 1 articles that cite this article, as of the time of this article download
- Access to high resolution figures
- Links to articles and content related to this article
- Copyright permission to reproduce figures and/or text from this article

View the Full Text HTML

J|A|C|S
COMMUNICATIONS

Published on Web 06/13/2008

Surface-Charge Induced Ion Depletion and Sample Stacking near Single Nanopores in Microfluidic Devices

Kaimeng Zhou, Michelle L. Kovarik, and Stephen C. Jacobson*

Department of Chemistry, Indiana University, 800 East Kirkwood Avenue, Bloomington, Indiana 47405-7102

Received April 12, 2008; E-mail: jacobson@indiana.edu

We report integrated nanopore/microchannel devices in which single nanopores are isolated between two microfluidic channels. The devices were formed by sandwiching track-etched conical nanopores in a poly(ethylene terephthalate) (PET) membrane between two poly(dimethylsiloxane) (PDMS) microchannels. Integration of the nanopores into microfluidic devices improves mass transport to the nanopore and allows easy coupling of applied potentials. Electrical and optical characterization of these individual nanopores suggests double layer overlap is not required to form an ion depletion region adjacent to the nanopore in the microchannel; rather, excess surface charge in the nanopore contributes to the formation of this ion depletion region. We used fluorescent probes to optically map the ion depletion region and the stacking of fluorescein near the nanopore/microchannel junction, and current measurements confirmed formation of the ion depletion region.

Our interest in nanofluidic devices stems from their unique ion and molecule transport characteristics,[1] demonstrated by a variety of experiments that have been conducted using protein and synthetic nanopores and nanochannels. Examples include single conical nanopores in track-etched membranes,[2] which have been used to sense individual porphyrin[3] and bovine serum albumin[4] molecules, and nanochannel devices, which efficiently concentrate fluorescein[5] and proteins and peptides[6,7] at the nanochannel/microchannel interface. These reports attribute this concentration effect to unbalanced ion flux through the nanochannel resulting from electrical double layer overlap in the nanochannel. Under such conditions, double layer overlap hinders electroosmotic flow[8] and co-ion transport, which, in turn, leads to concentration polarization when an electric field is applied.[9,10] This hindered ion transport has also been used to create chemical gradients across microfluidic layers separated by a high pore density membrane.[11] Similar devices incorporating recognition elements can concentrate mass-limited samples.[12] Conical nanopores are used to trap and concentrate particles electrokinetically due to the high electric field strength at the tips of the pores.[13,14] There are also a number of recent advances in fabrication of isolated solid-state nanopores,[15] which further provides opportunities for sensing applications and possibly DNA sequencing. In one example, individual nanopores are drilled into a silicon nitride/silicon oxide membrane using a transmission electron microscope, integrated with microfluidic channels, and combined with optical tweezers to measure the force exerted on translocating DNA molecules.[16] Isolation of single nanopores with microchannels provides an opportunity to probe electrokinetic and transport phenomena associated with nanoscale conduits. In the work presented here, we used track-etched membranes with multiple pores (10^6 pores/cm^2), which varied in their dimensions and conductance across a membrane. Consequently, isolation of individual nanopores within a membrane permitted us to determine how specific pores contributed to the formation of ion depletion regions and sample stacking.

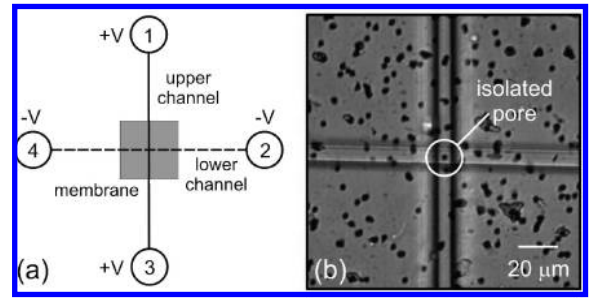

Figure 1. (a) Schematic of integrated nanopore/microchannel device. (b) Transmitted light image of two orthogonal microchannels isolating a single nanopore in the channel intersection. The black dots in the image are nanopores etched into the PET membrane.

Figure 1 shows a schematic of the assembled device and a transmitted light image of the membrane positioned between upper and lower microchannels. Conical nanopores in track-etched PET membranes[2] and PDMS microchannels[14] were fabricated as described previously. The nanopore dimensions measured with a scanning electron microscope were 130 ± 50 nm in diameter at the tip (n = 20) and 940 ± 110 nm in diameter at the base (n = 20). Each microchannel tapered to dimensions of 8.6 ± 0.6 μm wide and 18.6 ± 0.6 μm deep near the cross intersection (n = 5). Isolation of a single nanopore in the channel intersection was observed optically using transmitted light (see Figure 1b) and confirmed by electrical measurements. With no pores visible in the channel intersection, the conductance was zero, and with one pore isolated, the average conductance was 18.5 ± 8.3 nS with 10 mM phosphate buffer (n = 11 different pores).

Fluid transport was evaluated using an inverted optical microscope with an epifluorescence attachment, and a voltage source and picoammeter were used to measure the current as a function of applied potential and time. Initial experiments used a 10 μM fluorescein solution in 10 mM phosphate buffer with 100 mM NaCl. In the phosphate buffer (pH 6.8), the nanopore wall is negatively charged, and fluorescein is anionic so its electrophoretic mobility is opposite the electroosmotic mobility in the device. Additional device fabrication and characterization details are provided in the Supporting Information.

Figure 2 shows the formation of the ion depletion region with 5 V applied to reservoirs 1 and 3 with reservoirs 2 and 4 grounded (see Figure 1a). As seen in the fluorescence images, a depletion region forms on the anodic side of the nanopore in the vertical channel (Figure 2c,d). To verify formation of the ion depletion region, we conducted a series of current measurements to determine if the formation of the dark region coincides with a decrease in conductivity through the device. Figure 3a shows a set of current−voltage (I−V) curves for a single isolated nanopore. The applied potential was swept from 0 to 10 V in 0.5 V/step increments,

10.1021/ja802692x CCC: $40.75

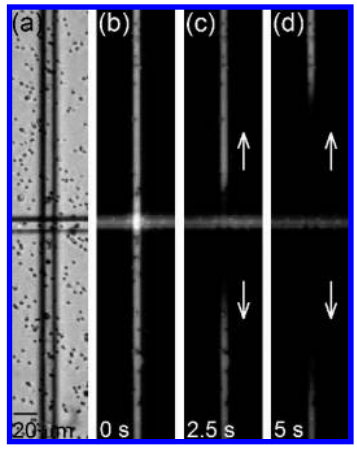

Figure 2. (a) Transmitted light image of the microfluidic device with a single nanopore isolated at the channel intersection. Fluorescence images of the ion depletion region forming in the vertical microchannel at (b) 0, (c) 2.5, and (d) 5 s after 5 V was applied to reservoirs 1 and 3 with reservoirs 2 and 4 grounded. Arrows depict direction of anionic transport. The buffer was 10 mM phosphate and 100 mM NaCl.

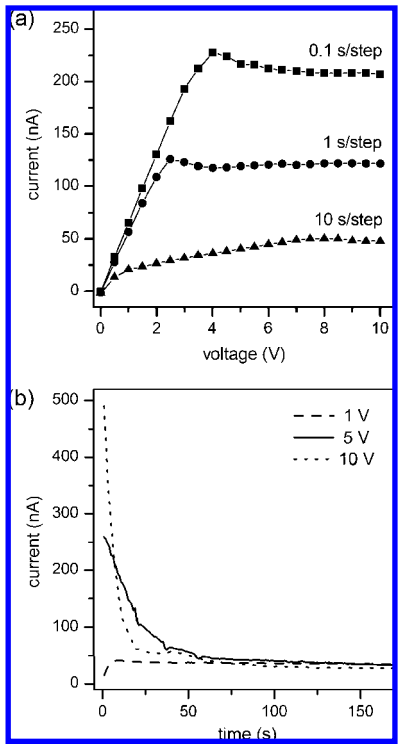

Figure 3. (a) Current−voltage ($I-V$) curves taken at 0.1, 1, and 10 s/step and (b) current−time ($I-t$) curves with 1, 5, and 10 V applied. Potentials were applied to reservoirs 1 and 3 with reservoirs 2 and 4 grounded. The buffer was 10 mM phosphate with 100 mM NaCl.

and the time for each step was 0.1, 1, or 10 s/step. As seen in Figure 3a, current and voltage follow an ohmic relation at low applied potentials, but a limiting current is reached at higher applied potentials. This $I-V$ behavior suggests that ions are indeed depleted near the intersection (Figure 2c,d), which limits the current passing through the microchannel. Results were identical when the positive potential was applied to either the tip or base side of the membrane, suggesting that the asymmetrical shape of the conical nanopore does not affect depletion region formation. Figure 3b shows current−time ($I-t$) curves when potentials of 0, 5, and 10 V were applied to the

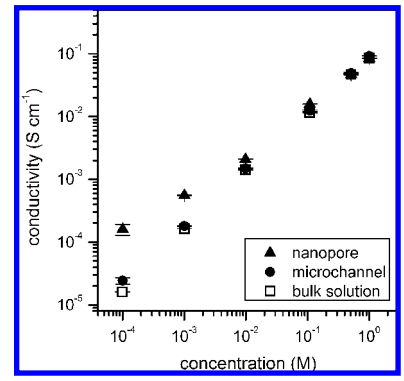

Figure 4. Variation of the conductivity in the nanopores, microchannels, and bulk solutions with buffer concentration. The error bars are $\pm\ \sigma$ for $n = 3$.

device for 5 min. With 5 and 10 V applied, the current drops significantly then remains constant, implying the formation of a stable ion depletion zone. With 1 V applied, no significant change in current with time is observed, indicating that no ion depletion zone forms. We attribute this to a threshold potential, which must be applied to overcome diffusion and enable an ion depletion region to form. With 1 V applied, diffusive transport within the microchannel is the same magnitude as the electrokinetic transport. However, applied potentials of 5 and 10 V result in electrokinetic transport, which is substantially higher than diffusive transport for the time scale of these experiments. The relative rates of diffusive and electrokinetic transport are discussed in more detail in the Supporting Information.

For these experiments, the electrical double layer is thin (~1 nm)[17] compared to the nanopore dimensions (tip diameter of ~130 nm), making double layer overlap unlikely. This is consistent with our observation that transport of co-ions (anions) through the pore is not hindered, and enrichment of fluorescein is not observed on the cathodic side of the pore (see Figure 2c,d). We measured the conductivities of the buffer in the bulk solution, in the microchannels, and in the nanopores. Figure 4 shows the conductivities over a range of buffer concentrations. Because the exact dimensions of the nanopores were not known, we assumed the microchannel and nanopore conductivities were similar for the 10 mM phosphate buffer with 500 mM NaCl, that is, the conductivity of the nanopore for this buffer concentration arose entirely from bulk flow of ions through the pore with negligible contribution from the surface charge. These measurements were duplicated, and our assumption confirmed, using a 10 mM phosphate buffer with 1 M NaCl. This assumption allowed us to determine the product $d_t d_b/L$, where d_t is the tip diameter, d_b is the base diameter, and L is the pore length, and to calculate the nanopore conductivity at different buffer concentrations. As seen in Figure 4, the microchannel and bulk solution conductivities were similar over the entire buffer concentration range, and the nanopore conductivities deviated from the microchannel and bulk conductivities at low buffer concentrations. This is due to the increased surface-to-volume ratio in the nanopore and, therefore, to an increased contribution to the nanopore conductivity from the surface charge. These conductivity measurements are described in more detail in the Supporting Information and are consistent with results reported for nanochannels in fused silica.[18] From the measurements at 10 mM phosphate buffer with 100 mM NaCl, we estimate that ~30% of the current is carried through the nanopore by the surface charge at this concentration. Consequently, the cation flux through the pore is larger than that in the microchannels, and the cations become depleted on the anodic

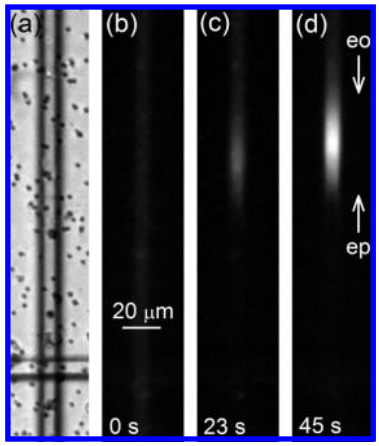

Figure 5. (a) Transmitted light image of the microfluidic device with a single nanopore isolated in the channel intersection. Fluorescence images of fluorescein concentration at (b) 0, (c) 23, and (d) 45 s after 5 V was applied to reservoir 1 with reservoir 2 grounded. Arrows show the direction of electroosmotic (eo) and electrophoretic (ep) transport.

side of the pore. Electroneutrality is maintained in this region by a decrease in the anion concentration.

In addition to an ion depletion region forming, we observe concentration of fluorescein in the microchannel due to stacking.[19] Figure 5 shows a series of fluorescence images taken 0, 23, and 45 s after the potential is applied to the device. The ion depletion region has a higher electric field strength than the rest of the microchannel, and fluorescein stacks at the anodic boundary of the depletion zone. The electrophoretic velocity is influenced by the local electric field strength in the depletion region, whereas the electroosmotic flow is averaged over the entire microchannel due to fluid incompressibility. Stacking also occurs at lower buffer concentrations (e.g., 10 mM phosphate) but not at higher buffer concentrations (e.g., 10 mM phosphate with 500 mM NaCl), where the current carried by the excess surface charge is minimal, and a depletion region does not form. Because the stacking requires a balance between electroosmotic and electrophoretic transport, stacking is not observed when the electroosmotic flow is enhanced by adding a surfactant, such as sodium dodecyl sulfate. These transport and stacking experiments are described in more detail in the Supporting Information.

In conclusion, these results show that ion depletion and sample stacking can occur in nanoscale devices even in the absence of double layer overlap. In previous work,[7] ion depletion zones formed in devices with similar geometries (40 nm deep channels), and the authors attribute the formation of the depletion zone to double layer overlap when the buffer concentration was low (e.g., $\leq$1 mM) and induced double layer overlap shortly after the application of the electrical potential when the buffer concentration was high (e.g., $\geq$10 mM). In our experiments, we do not observe conditions where double layer overlap is induced. For example, in the current−time profiles in Figure 3b, a 10-fold decrease in current occurs with the application of 10 V to the device. A 10-fold decrease in current corresponds to a 10-fold decrease in buffer conductivity and a 3-fold increase in the local double layer thickness from 1 to 3 nm. With a 3 nm double layer thickness in a 130 nm diameter tip, overlap is not expected. In addition, we did not observe the onset of overlimiting currents in our devices, in part, due to the range of applied potentials, buffer concentrations, and nanopore and microchannel dimensions used. Overall, our experiments demonstrate that transport anisotropies can arise under conditions of excess surface charge within the nanopore.

Acknowledgment. This work was supported in part by NSF CHE-0750295, by the Indiana METACyt Initiative of IU, funded in part through a major grant from the Lilly Endowment, Inc., and under a NSF Graduate Research Fellowship for M.L.K.

Supporting Information Available: Device fabrication and operation details and additional data from the conductivity, transport, and stacking experiments. This material is available free of charge via the Internet at http://pubs.acs.org.

References

(1) Holtzel, A.; Tallarek, U. *J. Sep. Sci.* **2007**, *30*, 1398–1419.
(2) Apel, P. Y.; Korchev, Y. E.; Siwy, Z.; Spohr, R.; Yoshida, M. *Nucl. Instrum. Methods Phys. Res. Sect. B* **2001**, *184*, 337–346.
(3) Heins, E. A.; Siwy, Z. S.; Baker, L. A.; Martin, C. R. *Nano Lett.* **2005**, *5*, 1824–1829.
(4) Sexton, L. T.; Horne, L. P.; Sherrill, S. A.; Bishop, G. W.; Baker, L. A.; Martin, C. R. *J. Am. Chem. Soc.* **2007**, *129*, 13144–13152.
(5) Pu, Q.; Yun, J.; Temkin, H.; Liu, S. *Nano. Lett.* **2004**, *4*, 1099–1103.
(6) Wang, Y. C.; Stevens, A. L.; Han, J. *Anal. Chem.* **2005**, *77*, 4293–4299.
(7) Kim, S. J.; Wang, Y. C.; Lee, J. H.; Jang, H.; Han, J. *Phys. Rev. Lett.* **2007**, *99*, 044501.
(8) Rice, C. L.; Whitehead, R. *J. Phys. Chem.* **1965**, *69*, 417–424.
(9) Rubinstein, I.; Shtilman, L. *J. Chem. Soc., Faraday Trans. 2* **1979**, *75*, 231–246.
(10) Tanaka, Y. *J. Membr. Sci.* **1991**, *57*, 217–235.
(11) Fa, K.; Tulock, J. J.; Sweedler, J. V.; Bohn, P. W. *J. Am. Chem. Soc.* **2005**, *127*, 13928–13933.
(12) Kim, B. Y.; Swearingen, C. B.; Ho, J. A. A.; Romanova, E. V.; Bohn, P. W.; Sweedler, J. V. *J. Am. Chem. Soc.* **2007**, *129*, 7620–7626.
(13) Lee, S.; Zhang, Y. H.; White, H. S.; Harrell, C. C.; Martin, C. R. *Anal. Chem.* **2004**, *76*, 6108–6115.
(14) Kovarik, M. L.; Jacobson, S. C. *Anal. Chem.* **2008**, *80*, 657–664.
(15) Dekker, C. *Nat. Nanotechnol.* **2007**, *2*, 209–215.
(16) Keyser, U. F.; van der Does, J.; Dekker, C.; Dekker, N. H. *Rev. Sci. Instrum.* **2006**, *77*, 105105.
(17) Bard, A. J.; Faulkner, L. R. *Electrochemical Methods*; John Wiley and Sons: New York, 1980.
(18) Stein, D.; Kruithof, M.; Dekker, C. *Phys. Rev. Lett.* **2004**, *93*, 035901.
(19) Burgi, D. S.; Chien, R.-L. *Anal. Chem.* **1991**, *63*, 242–2047.

JA802692X